
ATMOSPHERE AND HYDROSPHERE
PHYSICS

On the Structure of Temperature Pulsations near the Surface under Convective Conditions

E. A. Malinovskaya^{a,*}, O. G. Chkhetiani^a, and G. V. Azizyan^a

Presented by Academician G.S. Golitsyn December 23, 2023

Received December 23, 2023; revised January 29, 2024; accepted February 5, 2024

Abstract—Temperature pulsations are measured under conditions of summer hot weather in the near-surface air layer in a desert territory using wire sensors distributed spatially and in height with a recording frequency of 1000 Hz. For the power spectra, slopes with values from “−1” to “−1.35” (scales: 0.2–2 m) are recorded for frequencies below the “−5/3” inertial interval region. At frequencies above the inertial interval (scales: 0.01–0.1 m), slopes range from “−4.2” to “−5.8.” In some episodes at frequencies less than 0.1–0.3 Hz, there are slopes from “−0.2” to “−0.85.” Based on the equations of motion in the Boussinesq approximation, estimates are obtained for the observed slopes of the spectra: “−1,” “−4/3,” and “−7/3” that are typical of a thermally stratified medium. Using a qualitative (visual) method at different signal averaging times (1, 10, 200 s), the emergence of thermoconvective ramp structures with a temporal length of 0.3–1 s is revealed, which constitute a ramp with a length of 1–10 s at larger averaging.

Keywords: convection, temperature pulsations, turbulence spectra, ramp structures

DOI: 10.1134/S1028334X24601159

INTRODUCTION

Convection above a heated surface appears as a result of the ascent of warmer air masses (plumes) [1]. The density of distribution of convective elements is related to temperature pulsations [2] and the concentration of dusty aerosol. The pulsations of the vertical velocity component intensify with height [3], and there is an increasing correlation between pulsations of airflow velocity and temperature [4]. The measured data, both temperature and velocity exhibit triangular sawtooth spikes, termed “ramps” [5], which are visually noticeably separated from each other [6]. The sizes and distribution of ramps for temperature pulsations gives us an idea of structures in the convective heat flux [7]. The constantly occurring convective eddy structures ensure the main heat transfer and release of submicron aerosol under conditions of strong heating of a surface in desert areas.

Studying the statistical properties of pulsating components allows us to clarify the role of various dynamic mechanisms of structure forming. Among the main characteristics there are spectra of distributing velocity and temperature pulsations at frequencies (scales).

The range of scales where classical “−5/3” slopes are observed is limited [8]. The spectral slopes noticeably differ for the logarithmic, dynamic-convective sublayers, and the free convective sublayer [8] in the atmospheric boundary layer (ABL) at heights up to 50 m and demonstrate the slopes of “−1” and “−5/3.”

According to the SABLES98 observations, the lower atmosphere above flat homogeneous terrain had spectra where the segment of “−5/3” was preceded by both smaller and larger slopes under stable and unstable stratification conditions [9]. A “−2/3” spectrum was observed under natural convective conditions in the plantless territory when the measurements were taken at heights from 1.5 m to 30 m [10]. The different spectra constructed for the field measurement data are mentioned [11].

The theoretical estimates of power spectra show that under different conditions, slopes of −5/3, −1, −(2–5) ([12]) and −1, −4/3 ([13]), −5 [14] are likely to occur.

We note that the known measurements of natural convection were mostly conducted at heights greater than 1.5 m over the surface above various territories under moderately warm weather conditions (spring–early summer) (e.g., [8–10]).

This work studies statistical properties of pulsation components of temperature under convective conditions measured at heights of 20 and 80 cm during sum-

^a Obukhov Institute of Atmospheric Physics,
Russian Academy of Sciences, Moscow, 119017 Russia
*e-mail: elen_am@inbox.ru

mer with the surface heated to 30–50°C on desert sandy terrains devoid of vegetation.

The second section describes the territory and measurement procedure, as well as the factors affecting the obtained results such as dependences on time of day and the arrangement of measurement sensors. The third section compares the spectra of temperature pulsations for different conditions: clear sky, cloud cover, height, and position on the dune (shade, peak). The fourth section provides estimates explaining the observed slopes for the pulsation spectra near the heated surface. The fifth section contains a qualitative visual analysis of how self-similar convective structures appeared.

During the comprehensive field research of Obukhov Institute of Atmospheric Physics, Russian Academy of Sciences, conducted in the Chernozemelsky District of the Republic of Kalmykia in 2022, temperature and velocity pulsations were determined in addition to measuring aerosol fluxes and meteorological variables [2]. This region (Caspian Lowland) is characterized by typical semidesert landscapes with extensive sandy areas where a stable dune relief is formed. A developed wireless pulsation measuring complex in use included six alternating current thermometers and six constant temperature thermoanemometers based on wire sensors made of gold-coated tungsten 10 μm wire. The frequency of recording the data from the pulsation sensors corresponds to 1000 Hz. The studies were conducted under natural conditions; therefore, when data were chosen for analysis, the cloud cover effect and surface orography were taken into account: the appearance of turbulent structures in flowing around and shading areas at a change in solar incidence angle (inhomogeneity of temperature distribution). The surface is heated in the morning hours up to 25–26°C with a surface temperature gradient of up to 9°C, reaching 66°C by the evening and a temperature gradient of 30°C ([15], Fig. 3).

In 2022, the dunes were arranged at the measurement site so that one of their slopes was in the shade, while the other was heated by the sun; the shaded areas appeared in the time intervals from 8:00 a.m. to 11:00 a.m. and from 3:00 p.m. to 6:00 p.m. (Fig. 2). For the sunny and shady slopes, the temperature difference reaches 6 degrees from 9:00 a.m. to 11:30 a.m. at a height of 20 cm. The maximum air temperatures were close to 39°C in the measurement campaign of 2022.

According to the dynamics of incident radiation flux, for three days of observations (July 22, July 28, and July 29), there was no cloud cover on July 22 and July 29. On July 28, special time intervals with solar radiation incidence were recorded from 10:00 a.m. to 10:30 a.m. and from 11:30 a.m. to 12:00 p.m.

These different states are taken into account in the presented research.

The spectra were constructed for 20-min intervals for the pulsation components of temperature, deter-

mined after subtracting a 2-min average selected for this task. When selecting, the averages were considered with an increase in frequency interval from 0.02 to 1 Hz at a shift towards higher values.

In analyzing the spectra, we assume that the random thermal eddy structures forming them are generated by the heated surface, and their (observed) sizes depend on:

- the location on the dune (shade, peak);
- the height of the sensor relative to the surface;
- are affected by cloud cover.

For three points with distributed measurements on distributed masts at 12:00 p.m. and 5:00 p.m., we observe similar spectral structures (Fig. 3a, 3b) for the different points. Discrepancies are recorded better when temperature differences appear, as shown for 5:00 p.m. (Fig. 3b).

Temperature pulsation spectra at different heights of 20 and 80 cm have a similar structure (Figs. 3c–3f). Discrepancies appear after the interval with the passage of cloud cover on July 28 at 12:00 p.m. (Fig. 3c) and on the sunny day of July 29 at 11:00 a.m. (Fig. 3f) when significant temperature variations are recorded.

Three spectral ranges with inflections in the frequency range ω : 0.1–1, 10–200 Hz are distinguished. This corresponds to the intervals of 0.1–10 s and 0.005–0.01 s (Fig. 3). The slope exponents in the first two ranges are “–1” and “–5/3,” respectively. The slope exponent in the third range varies from –2.5 (–7/3) to –5.5 (–17/3). There are episodes at frequencies <0.1–0.3 Hz when slopes from “–0.2” to “–0.85” are present.

The slopes close to “–5/3” change insignificantly during the day (Fig. 4b). For the exponents close to “–1” (Fig. 4a), significant discrepancies in values (by 20%) are recorded on a cloudy day in the afternoon; at a height of 20 cm, the slope is “–1,” and at a height of 80 cm, it is “–4/3” (~–1.3). For a clear day, the values at the heights of 20 and 80 cm differ by 3–10%. The largest difference is recorded at around 12:00 p.m., the exponents are the closest to “–1.” At other times, they vary from –1.1 to –1.2.

Using the data from the acoustic thermoanemometer placed at a height of 2 m, the dynamic velocity was determined for each time moment. Wind velocity were estimated at heights of 20 and 80 cm to the logarithmic profile approximation. The estimates of the scales for turbulent structures carried by the wind are made based on the hypothesis of frozen turbulence. Figures 4c, 4d show the time variation of typical scales for the estimated velocity values at 20 and 80 cm elevations. For temperature spectra in the vicinity of the first inflection, the scales vary from 0.2 to 2 m during the day at the frequencies from 1 to 20 Hz (0.05–1 s). Maximum frequencies appear here from 11:00 a.m. to 1:00 p.m. For the vicinity of the second inflection in the spectra, there are frequencies of 50–150 Hz

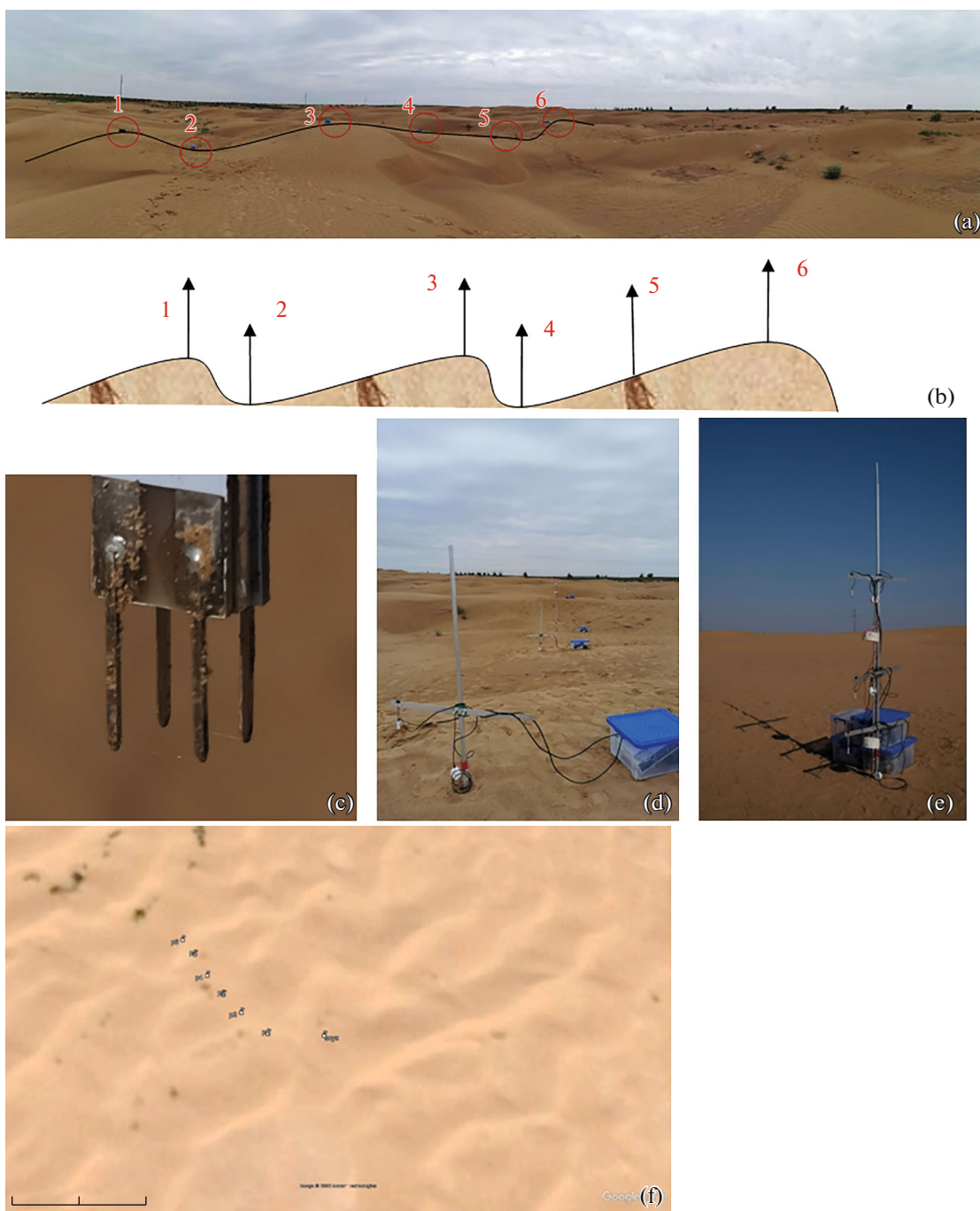


Fig. 1. Layout pattern of the 2-m masts and placement of the sensors from the pulsation measuring wireless complex (panorama, along the line, nearby, in the satellite image) and illustration of implementing the second experiment with the sensors at different heights.

(0.007–0.02 s), which corresponds to the scales of 0.01–0.1 m.

The dynamics of the change in structure sizes during the day is shown for the cloudless day of July 29 with gentle wind for two vicinities of inflections in the spectrum. Maximum wind velocity were recorded at 2:00 p.m., when the largest typical scales and the largest scale range for the inflection near the exponent “–1”

appeared, which is caused by the increased wind action. At other times, the wind velocity varied within 20%. At 11:00 a.m., which is a special moment related to continuous non-uniform surface heating (shade from dunes), scales significantly differed for the inflection near the slope exponent “–5/3,” which may be associated with the emergence of thermal wind near the surface.

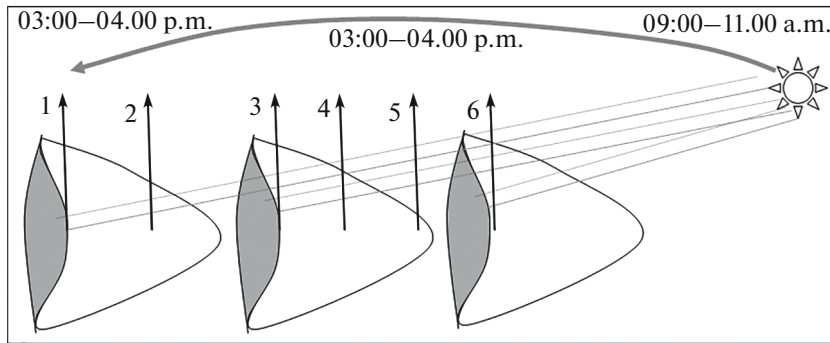


Fig. 2. Variation in the angle of incidence of sunlight on the surface (Sun's path scheme).

In the vicinity of the first inflection (Fig. 4c), the largest difference is observed at 2:00 p.m., which is likely related to the scattering of thermal structures ascending from the well-heated surface. For the vicinity of the second inflection, the differences in scales (Fig. 4d) at 11:00 a.m. may be related to the intensified horizontal flux near the surface due to inhomogeneous heating.

We consider that the relatively small change in the scale of the structure with height may be due to wind transport, while significant differences may be related to heat-flux dispersion or the presence of horizontal heat fluxes.

We mention the temperature pulsation spectra obtained by processing experimental field records: “-5/3” in the inertial range, close to “-1”- “-1.3” and to “-0.2”-“0.8” at low frequencies, and close to “-4.2”-“-5.8” in the dissipative range. The next section provides the analysis of appearance of possible spectral slope exponents.

To study flows over a heated surface, we use the equations of motion in the Boussinesq approximation. The ascending heated, warmer air is described by the equations:

$$\frac{\partial v_i}{\partial t} + v_j \frac{\partial v_i}{\partial x_j} = -\frac{1}{\rho_0} \frac{\partial p}{\partial z} + \nu \frac{\partial^2 v_i}{\partial x_i^2} - g\beta\theta e_3, \quad (1)$$

$$\frac{\partial \theta}{\partial t} + v_i \frac{\partial \theta}{\partial x_i} = \chi \frac{\partial^2 \theta}{\partial x_i^2}, \quad (2)$$

where θ is temperature change, χ is thermal conductivity coefficient, β is expansion coefficient, v_i is components of air flow velocity, and p, ρ_0 are density and pressure.

Taking into account the near-surface temperature gradient, we obtain the following relationships for the averaged pulsation components:

$$\frac{\langle \theta^2 \rangle}{\tau} \sim \varepsilon_\theta + \langle v_z \theta \rangle \left| \frac{dT}{dz} \right|, \quad \frac{dT}{dz} < 0, \quad (3)$$

$$\frac{\langle v_z \theta \rangle}{\tau} \sim \varepsilon_{v_z \theta} + \langle v_z^2 \rangle \left| \frac{dT}{dz} \right| + \beta g \langle \theta^2 \rangle, \quad (4)$$

$$\frac{\langle v_z^2 \rangle}{\tau} \sim \varepsilon_z + \beta g \langle v_z \theta \rangle. \quad (5)$$

In the equations for $\langle v_z \theta \rangle$ and $\langle v_z^2 \rangle$, dissipation can be neglected on large scales. The main source for $\langle v_z \theta \rangle$ is the temperature gradient; therefore, $\beta g \langle \theta^2 \rangle$ can be omitted here. At the same time, for temperature pulsations, the main factor is the rate of smoothing of thermal inhomogeneities, characterized by ε_θ .

Then

$$\frac{\langle \theta^2 \rangle}{\tau} \sim \varepsilon_\theta, \quad \frac{\langle v_z \theta \rangle}{\tau} \sim \langle v_z^2 \rangle \left| \frac{dT}{dz} \right|, \quad \frac{\langle v_z^2 \rangle}{\tau} \sim \beta g \langle v_z \theta \rangle. \quad (6)$$

Hence,

$$\tau \sim \left(\beta g \left| \frac{dT}{dz} \right| \right)^{-1/2} = N^{-1}, \quad (7)$$

where $N^2 = \beta g \left| \frac{dT}{dz} \right|$ is the Brunt-Väisälä frequency squared, which does not depend on scale in this case. This is a typical time scale for the exponential growth (or fluctuations) of thermal inhomogeneities in the presence of a temperature gradient.

Consequently, $\langle \theta^2 \rangle \sim \frac{\varepsilon_\theta}{N}$, and for the spectrum

$\langle \theta^2 \rangle = \int F_k dk$ we obtain

$$F_k \sim \frac{\varepsilon_\theta}{N} k^{-1}. \quad (8)$$

Note that here the situation is in a certain way similar to the turbulence of a flow with a transverse shear $U = (Sz, 0, 0)$, where such a spectrum is also obtained at large scales and low frequencies. It is exactly in this range that submesoscale structures are observed in the atmospheric boundary layer [16], which is clearly

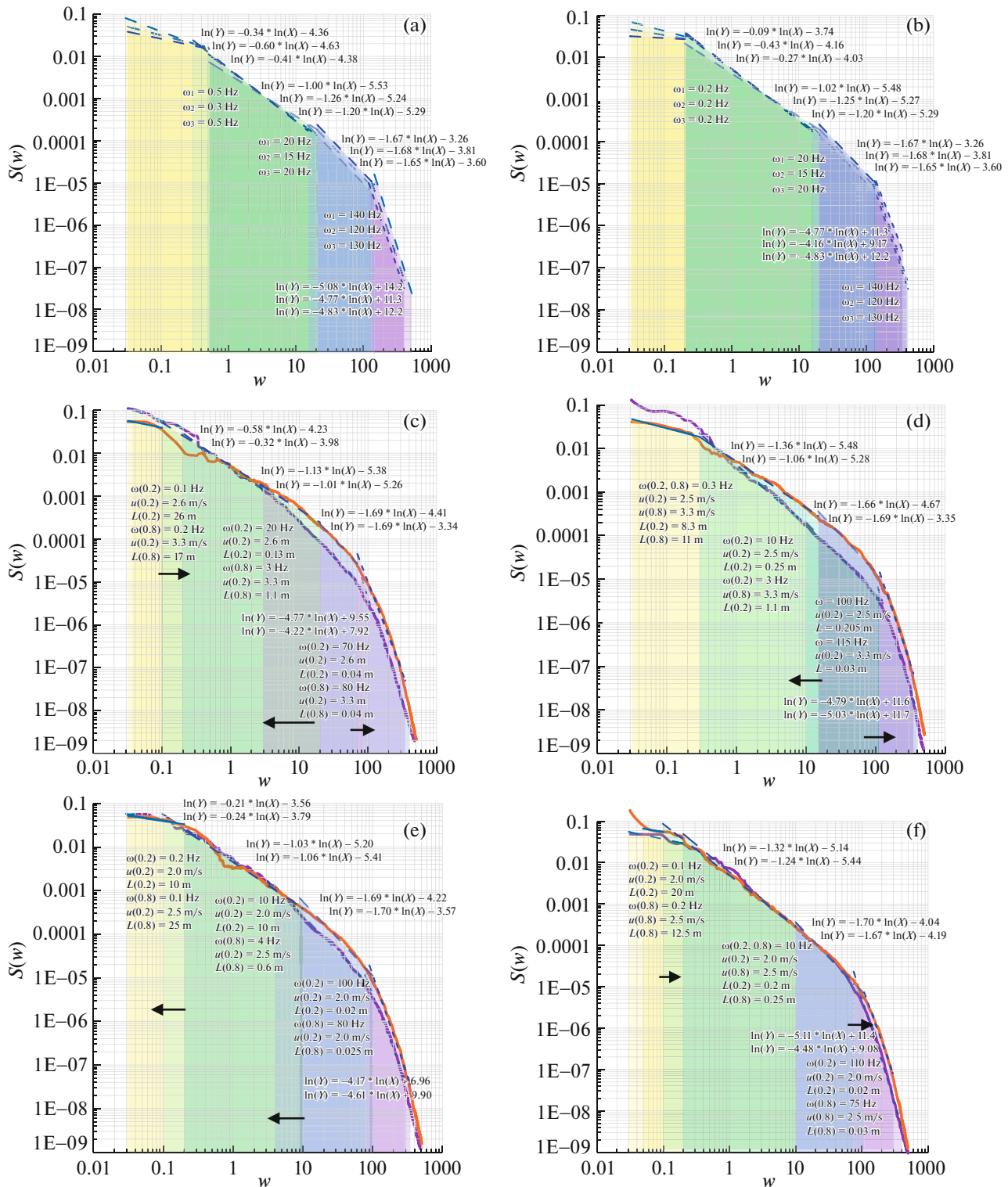


Fig. 3. Spectra of temperature pulsations: (a) July 22 at 12:00 p.m. points 1–3; (b) July 22 at 1:00 p.m. points 1–3, (c) July 28 at 12:00 p.m. at heights of 20 and 80 cm, (d) July 29 at 1:00 p.m. at heights of 20 and 80 cm, (e) July 28 at 10:00 a.m. at heights of 20 and 80 cm, (f) July 29 at 11:00 a.m. at heights of 20 and 80 cm (ω is frequency, $u(20)$).

expressed for turbulence spectra [8]. Theoretically, slope “-1” was obtained in [13] in the presence of wind shift and temperature gradient; in neglecting turbulent mixing (in [12] and in [8] on the assumption of

height independence of the sizes of turbulent large eddies). The “-1” spectrum is recorded in a thermally stratified medium for the low-m/s range, where mixing is less active [17].

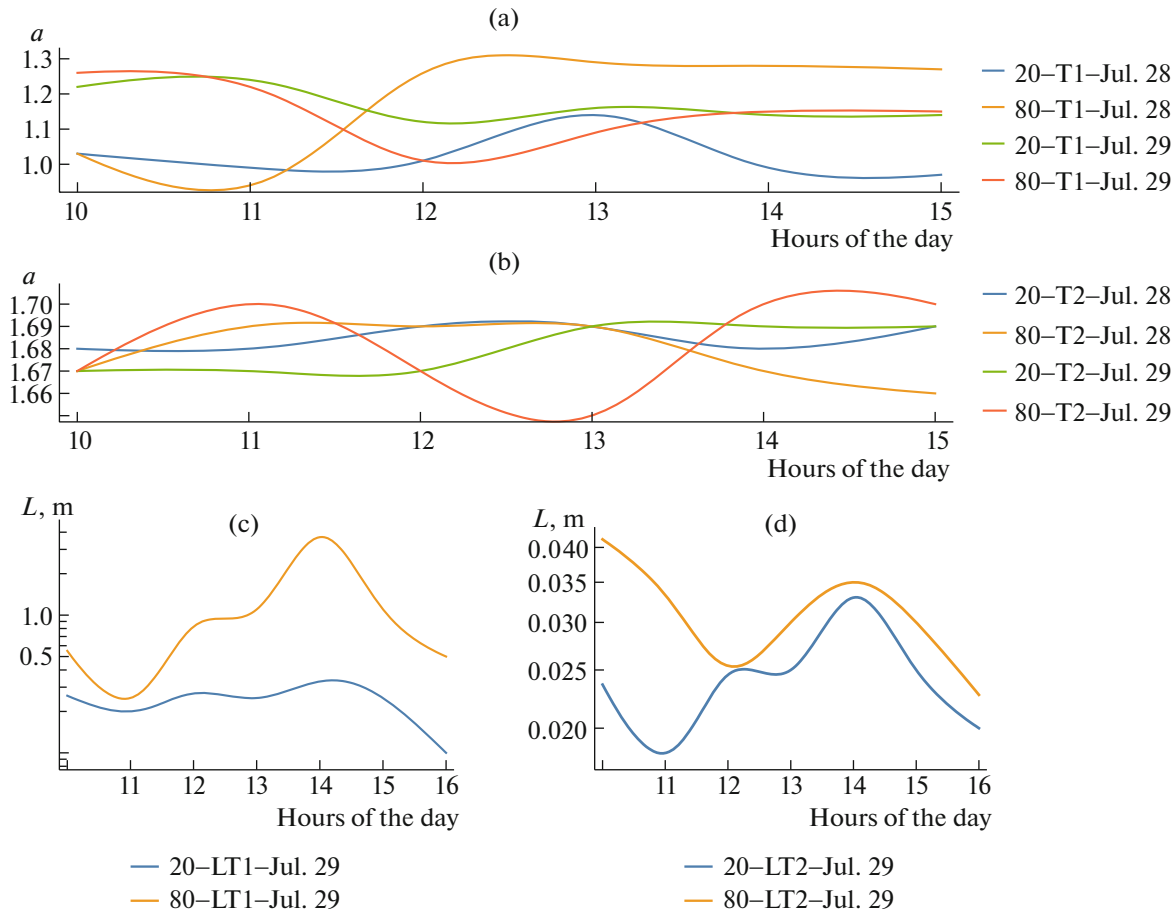


Fig. 4. Dynamics of changes in structure scales ((a) the first inflection point, (b) the second inflection point) on a clear day on July 29, 2022, and frequencies on July 28, 2022 and July 29, 2022 at the inflection points, changes in slope exponents during the day on July 28 and July 29 (square areas designate moments with cloud cover on July 28).

To implement the regime of such a spectrum, it is necessary to satisfy the inequality $\tau < \tau_{kolm}$, where τ_{kolm} is the typical time in the inertial interval

$$\tau_{kolm} \sim \frac{l}{v_l} = \frac{l}{\epsilon^{1/3} l^{1/3}} = \frac{l^{2/3}}{\epsilon^{1/3}}. \quad (9)$$

Hence, we obtain that the -1 spectrum can be observed at scales

$$l > \epsilon^{1/2} \left(\beta g \left| \frac{dT}{dz} \right| \right)^{-3/4}. \quad (10)$$

With the surface heating up to 60–70 degrees and a temperature drop by 20–30 degrees in the first 10 cm, energy dissipation of about 0.05 m²/s³, $l > 5-7$ cm. That is, such a spectrum in the near-surface air layer above a well-heated surface (under arid conditions) can be definitely observed at scales of 10 cm and more. At smaller scales, the spectrum should be $-5/3$.

In the other limiting case, the turbulent heat flux $\langle v_z \theta \rangle$ depends only on energy dissipation. Temperature pulsations depend on the rate of smoothing of

thermal inhomogeneities $\frac{\langle \theta^2 \rangle}{\tau} \sim \epsilon_\theta$. The pulsations of the vertical component in turbulent energy $\langle v_z^2 \rangle$ depend, in turn, on the heat flux magnitude $\langle v_z \theta \rangle$. Then we obtain the following estimate expressions:

$$\frac{\langle \theta^2 \rangle}{\tau} \sim \epsilon_\theta, \quad \frac{\langle v_z \theta \rangle}{\tau} \sim \epsilon_{v_z \theta}, \quad \frac{\langle v_z^2 \rangle}{\tau} \sim \beta g \langle v_z \theta \rangle. \quad (11)$$

Hence, $\langle v_z^2 \rangle \sim \beta g \epsilon_{v_z \theta} \tau^2$ and

$$\langle \theta^2 \rangle \sim \frac{\epsilon_\theta \langle v_z^2 \rangle^{1/2}}{(\beta g \epsilon_{v_z \theta})^{1/2}} \sim \frac{\epsilon_\theta \epsilon^{1/3} l^{1/3}}{(\beta g \epsilon_{v_z \theta})^{1/2}}. \quad (12)$$

Consequently, for the spectrum, we have an estimate:

$$F_k \sim \frac{\epsilon_\theta \epsilon^{1/3}}{(\beta g \epsilon_{v_z \theta})^{1/2}} l^{-4/3}. \quad (13)$$

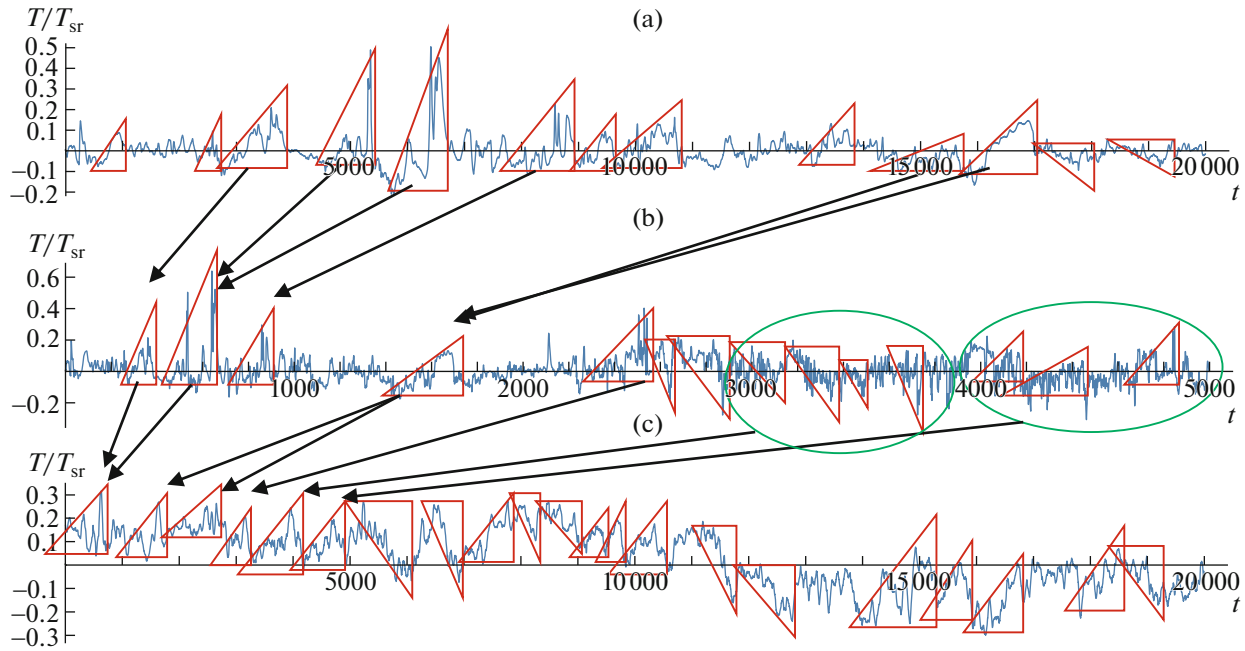


Fig. 5. Manifestation of self-similarity of structures at a change in visualization and averaging scales. (a) Representing on the 20-s interval, 1-s averaging, highlighted structures have lengths from 300 to 1000 ms; b) representing on the 50-s interval with $\times 10$ coefficient, 10-s averaging, highlighted structures have lengths from 1 to 3 s; (c) representing on the 50-s and 200-s intervals, 100-s averaging, structures have lengths from 1 to 10 s.

We note the observations of the spectrum with a slope “-1.2” in the evening when the stratification of the near-surface layer is weakening in the atmospheric boundary layer in [18].

In the equations for $\langle v_z \theta \rangle$ and $\langle v_z^2 \rangle$, we take into account dissipation on large scales. The main source for temperature pulsations is the temperature gradient, as well as the heat flux $\langle v_z \theta \rangle$. Then we obtain estimates under conditions of dissipation and significant temperature gradient:

$$\frac{\langle \theta^2 \rangle}{\tau} \sim \langle v_z \theta \rangle \left| \frac{dT}{dz} \right|, \quad \frac{\langle v_z \theta \rangle}{\tau} \sim \varepsilon_{v_z \theta}, \quad \frac{\langle v_z^2 \rangle}{\tau} \sim \varepsilon_z. \quad (14)$$

Hence,

$$\langle \theta^2 \rangle \sim \varepsilon_{v_z \theta} \frac{l^{4/3}}{\varepsilon^{2/3}} \left| \frac{dT}{dz} \right|. \quad (15)$$

For the spectrum, we obtain

$$F_k \sim \frac{\varepsilon_{v_z \theta}}{\varepsilon^{2/3}} \left| \frac{dT}{dz} \right| l^{-7/3}. \quad (16)$$

The inhomogeneities of the natural eolian surface contribute to the emergence of small-scale local convective and turbulent structures. These inclined vertical structures are pushed by the wind. As a result, the measurement data have spikes with a typical structure called a ramp. Since ramp structures are self-similar, their various sizes L_r can be identified for different

time averaging intervals Δt_i and the selected interval of visual representation L_r . Averaging over large intervals leads to their blurring. If $\Delta t_i < L_r$, averaging is performed excluding the trends of its slope; when $\Delta t_i \approx L_r$ up to half of the amplitude value is lost; when $\Delta t_i > L_r$ the structures are visible. Averaging over 1 s (Fig. 5a) shows ramps with lengths of 300–1000 ms, that integrate into larger ones ~ 1 s in size in averaging over 10 s (Fig. 5b). During the transition from 10-s to 200-s averaging, ramps also increase in size by a factor of 10. An interesting effect is noted in Fig. 5 where upon integration, the descending ramps formed a larger ascending ramp, which indicates inhomogeneity of thermal structures.

During such a visual examination, we observe that merging and enlargement of structures affect the change in statistical characteristics.

The characteristics of the ramp structures at a low height up to 2 m under conditions of convective instability during summer with the surface heated to 30–50°C under arid conditions in the absence of vegetation were studied using visual and statistical methods.

Based on the data from two experiments for the distributed (different temperature regimes) and multi-level (development of thermocurrent structure with height) placement of the sensors, we compared spectral density functions.

The analysis of the temperature pulsation spectra showed that their structure is affected by

- the location on the dune (shade, peak);
- cloud cover;
- wind velocity;
- temperature regime.

In the plots (Fig. 3), there are four linear segments with exponents “ <-1 ,” “ -1 ” (“ -1.3 ”), “ $-5/3$ ” and “ -4 ”–“ -6 .” Frequency intervals in the vicinity of the inflection correspond to 0.1–0.5, 1–20, and 100–130 Hz.

The typical scales of the structures were calculated based on the theory of frozen turbulence, they varied from 0.2 to 2 m and from 0.02 to 0.1 m for the upper and lower vicinities of the inflection points near the “ $-5/3$ ” inertial interval.

The exponents in the vicinity of the first inflection are close to “ -1 ” for meter-sized structures, typical of hot daytime after the surface is heated under light and shade conditions. The exponents from “ -1.1 ” to “ -1.3 ” characterize less heated air in cloud conditions for small scales from 0.1 to 0.6 m.

The exponent “ -1 ” is related to the presence of thermal inhomogeneities and appreciable temperature gradient. The exponent “ $-4/3$ ” is determined by the requirement to preserve thermal inhomogeneities that generate turbulent pulsations.

We note the unity of dynamic processes forming the observed spectral structure of turbulence pulsation characteristics at different scales — from the troposphere [12, 19], the atmospheric boundary layer [8, 20], and directly in the near-surface convective layer.

The visual analysis of relative changes in the temperature pulsation components revealed the presence of triangular asymmetric structures (“ramps”). Their size depends on the averaging interval, varies from 300 ms to 10 s; the cases of structure self-similarity are recorded upon their comparison.

ACKNOWLEDGMENTS

We are grateful to L.O. Maksimenkov, E.A. Shishov, and B.A. Khartskhaev (Komsomolsky, Kalmykia) for their assistance in organizing and conducting in-situ measurements. We thank G.S. Golitsyn and E.B. Gledzer for their attention to this work and constructive feedback.

FUNDING

This work was supported by the Russian Science Foundation (project no. 20-17-00214).

CONFLICT OF INTEREST

The authors of this work declare that they have no conflicts of interest.

REFERENCES

1. R. Krishnamurti and L. N. Howard, *Proc. Natl. Acad. Sci.* **78** (4), 1981–1985 (1981).
2. E. A. Malinovskaya, O. G. Chkhetiani, G. S. Golitsyn, and V. A. Lebedev, *Dokl. Earth Sci.* **509** (2), 222–230 (2023).
3. A. S. Frisch and J. A. Businger, *Boundary Layer Meteorol.* **3** (3), 301–328 (1973).
4. B. M. Koprov et al., *Boundary Layer Meteorol.* **88** (3), 399–423 (1998).
5. R. J. Taylor, *Aust. J. Phys.* **11** (2), 168–176 (1958).
6. W. Chen et al., *Boundary Layer Meteorol.* **84**, 99–124 (1997).
7. D. Phong-Anant, A. J. Chambers, and R. A. I. Antonia, in *Proc. Australasian Conf. on Hydraulics and Fluid Mechanics* (ACT, Barton, 1980), Vol. 7, pp. 432–434.
8. B. A. Kader, *Izv. Akad. Nauk SSSR, Fiz. Atmos. Okeana* **28** (12), 1235–1250 (1988).
9. J. M. Vindel and C. Yagüe, *Boundary Layer Meteorol.* **140**, 73–85 (2011).
10. K. G. McNaughton, R. J. Clement, and J. B. Moncrieff, *Nonlin. Process. Geophys.* **14** (3), 257–271 (2007).
11. G. I. Gorchakov, O. G. Chkhetiani, A. V. Karpov, R. A. Gushchin, and O. I. Datsenko, *Dokl. Earth Sci.* (2024) (in press).
12. C. P. Martens, *J. Phys. A* **9–10**, 1751–1770 (1976).
13. F. A. Gisina, *Tr. Leningrad. Gidrometeorol. Inst.*, No. 34, 49–58 (1968).
14. A. G. Sazontov, *Izv. Akad. Nauk SSSR, Fiz. Atmos. Okeana* **15** (8), 820–828 (1979).
15. O. G. Chkhetiani, E. B. Gledzer, M. S. Artamonova, and M. A. Iordanskii, *Atmos. Chem. Phys.* **12**, 5147–5162 (2012).
16. O. G. Chkhetiani and N. V. Vazaeva, *Izv., Atmos. Oceanic Phys.* **55** (5), 432–446 (2019).
17. T. M. Dillon and D. R. Caldwell, *J. Geophys. Res.: Oceans* **85**, 1910–1916 (1980).
18. G. S. Young, *Earth-Sci. Rev.* **25** (3), 179–198 (1988).
19. S. K. Kao, *J. Atmos. Sci.* **27** (7), 1000–1007 (1970).
20. F. A. Gisina, *Izv. Akad. Nauk SSSR, Fiz. Atmos. Okeana* **2** (8), 804–813 (1966).

Translated by L. Mukhortova

Publisher’s Note. Pleiades Publishing remains neutral with regard to jurisdictional claims in published maps and institutional affiliations.